


RESEARCH ARTICLE

Temperature influence on NiFeMo nanoparticles magnetic properties and their viability in biomedical applications

Fabio Muchenski¹ | Jenifer Pendiuk Gonçalves² | Yasmin Carla Ribeiro² |
 Célia Regina Cavichiolo Franco² | Carolina Camargo de Oliveira² |
 Bruna Hilzendeger Marcon³ | Anny Robert³ | Lia Carolina Soares de Medeiros³ |
 Ronei Cardoso de Oliveira⁴ | Adilson Jesus Aparecido de Oliveira⁴ | Ney Mattoso⁵ 

¹Instituto Federal Catarinense, São Bento do Sul, Brazil

²Cell Biology Department, Laboratory of Inflammatory and Neoplastic Cells/ Laboratory of Sulfated Polysaccharides Investigation, Biological Sciences Sector - Universidade Federal do Paraná, Curitiba, Brazil

³Cell Biology Laboratory, Instituto Carlos Chagas (Fiocruz - Paraná), Curitiba, Brazil

⁴Physics Department, Center for Exact Sciences and Technology, Superconductivity and Magnetism Laboratory, Universidade Federal de São Carlos, São Carlos, Brazil

⁵Physics Department, Exact Sciences Sector, Laboratory of Nanostructured Materials, Universidade Federal do Paraná, Curitiba, Brazil

Correspondence

Ney Mattoso, Departamento de Física, Setor de Ciências Exatas, Laboratório de Materiais Nanoestruturados, Universidade Federal do Paraná. Avenida Francisco H dos Santos, 100, Curitiba, CEP 81531-980, Brazil.
 Email: mattoso@ufpr.br

Funding information

Conselho Nacional de Desenvolvimento Científico e Tecnológico, Grant/Award Number: 312227/2021-3

Abstract

NiFeMo alloy nanoparticles were synthesized by co-precipitation in the presence of organic additives. Nanoparticles thermal evolution shows that there is a significant increase in the average size (from 28 to 60 nm), consolidating a crystalline structure of the same type as the Ni₃Fe phase but with lattice parameter $a = 0.362$ nm. Measurements of magnetic properties follow this morphological and structural evolution increasing saturation magnetization (Ms) by 578% and reducing remanence magnetization (Mr) by 29%. Cell viability assays on as-synthesized revealed that nanoparticles (NPs) are not cytotoxic up to a concentration of 0.4 µg/mL for both non-tumorigenic (fibroblasts and macrophages) and tumor cells (melanoma).

KEYWORDS

cell viability, co-precipitation, cytotoxicity, magnetic nanoparticles, organic additives

1 | INTRODUCTION

The use of magnetic nanoparticles for biomedical applications is not new.¹ Several works on Superparamagnetic Iron Oxide Nanoparticles (SPIONs) have been published. A review published by Wei et al.² provides a good overview of these nanoparticles, particularly magnetite (Fe₃O₄), and maghemite (γ-Fe₂O₃). Characteristics such as low cytotoxicity in general and superparamagnetic behavior² To obtain these superparamagnetic properties, SPIONs must have their size <20 nm typically to configure a single magnetic domain.³ SPIONs size can be an issue in terms of biocompatibility. Very small nanoparticles can be more easily internalized, becoming more cytotoxic than larger

particles.⁴ To resolve this problem, SPIONs are mounted in a structure known as a core-shell.⁵ Various materials of excellent biocompatibility are used to shelter SPIONs such as Polymers,⁶ SiO₂,⁷ and Au.⁸ Other nanoparticles from different magnetic materials are being studied, such as cobalt-nickel ferrites Co_xNi_{1-x}Fe₂O₄,⁹ nickel-iron ferrites NiFe₂O₄,¹⁰ nickel oxide NiO, and nickel hydroxide Ni(OH)₂.¹¹ In this work, we present the first results of NiFeMo alloy nanoparticles cellular viability aiming for future biomedical applications. In its massive form, this alloy has unique characteristics such as low coercive field (Hc), high saturation magnetization (Ms), and low remanence (Mr).¹² Literature shows that NiFeMo particles can be produced by high-energy ball milling,^{13,14} showing excellent magnetic properties, but

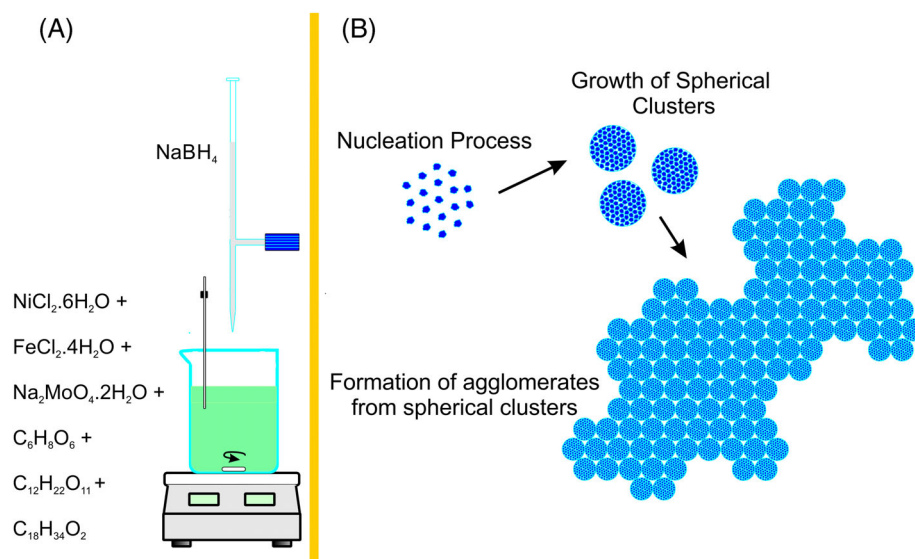


FIGURE 1 (A) schematic representation of nanoparticles synthesis, (B) illustration of particles microstructure evolution during synthesis.

the particles were micrometric, making their use for biomedical applications unfeasible. Our group recently reported the results on NiFeMo nanoparticles with sizes of 20–40 nm produced by co-precipitation in the presence of organic additives.¹⁵ In addition to being the first work in the literature that studies the cellular viability of this magnetic alloy in the form of nanoparticles, within our knowledge, we also present the results of these nanoparticles improvement by the effect of annealing temperature. Therefore, this work aims to contribute in two directions. The first is the issue of morphological and structural improvement as a function of subsequent thermal annealing, as well as the reflection of these changes in the magnetic properties of NiFeMo nanoparticles. The second aspect presented is about the cell viability of these nanoparticles in cells that can interact in a possible biomedical application. Thus, it is expected that these non-coated nanoparticles show potential for future applications in hyperthermia magneto with reducing internalization.

2 | MATERIALS AND METHODS

2.1 | Synthesis

The nanoparticles were produced by the co-precipitation technique. The following reagent grade components were used in 70 mL aqueous solution: nickel chloride ($\text{NiCl}_2 \cdot 6\text{H}_2\text{O}$) (80 mmol/L), iron chloride ($\text{FeCl}_2 \cdot 4\text{H}_2\text{O}$) (12 mmol/L), sodium molybdate ($\text{Na}_2\text{MoO}_4 \cdot 2\text{H}_2\text{O}$) (1 mmol/L), sucrose ($\text{C}_{12}\text{H}_{22}\text{O}_{11}$) (29 mmol/L), L-ascorbic acid ($\text{C}_6\text{H}_8\text{O}_6$) (14 mmol/L), oleic acid ($\text{C}_{18}\text{H}_{34}\text{O}_2$) (0.02 mmol/L) and sodium borohydride (NaBH_4) (10 mL). The synthesis was performed at room temperature under vigorous magnetic stirring and with 10 mL of NaBH_4 dripping. This process lasts for about 10 min and the solution remains under agitation for another 15 min. Figure 1A represents the experimental arrangement for nanoparticles synthesis. After completing the synthesis, the nanoparticles solution underwent a washing process. To remove residues of organic and inorganic additives,

washings were carried out with double-distilled water repeated 3 times and then with ethyl alcohol for another 10 times. Washes were performed by centrifugation at 7 krpm. After washing, the samples are placed in an oven at 60°C for 12 h. After drying, the samples are placed in a quartz tube furnace under N_2 flow ($1 \text{ cm}^3/\text{s}$) to avoid sample oxidation. The thermal annealing temperatures were 400, 600, 800, and 1000°C. These temperatures have reached a rate of 10°C/min and were held for 30 min at the indicated temperatures.

2.2 | Morphological, structural, and chemical characterization

Morphological characterization of the nanoparticles as-synthesized and heat treated was performed by TEM on a JEOL JEM 1200EX-II operating at 120 kV. Samples stored in the cell culture medium were analyzed in the TEM JEOL JEM 1400 Plus operating at 100 kV. For sample preparation, nanoparticles in an isopropyl alcohol suspension were dripped onto 200 mesh copper grids coated with formvar/carbon film. Structural characterization was performed by Selected Area Electron Diffraction (SAED) on the TEM JEOL JEM 1200EX-II. For camera constant calibration, a gold standard sample was used. Elementary chemical characterization was performed by Oxford EDS coupled to SEM TESCAN VEGA3 LMU operating at 15 kV. For EDS analysis, the samples were dispersed on a double-sided carbon tape attached to the aluminum stub, without the deposition of any gold or carbon film on the samples.

2.3 | Magnetic characterization

Magnetic properties of the nanoparticles were carried out in an EG&G Princeton Applied Research Model 4500 vibrating sample magnetometer (VSM) with a maximum magnetic field of 1.3T. Measurements were carried out at a temperature of 298 K. Before measurements,

the VSM was calibrated with a standard palladium sample provided by Quantum Design.

2.4 | Biological assays

2.4.1 | Materials

Neutral red dye and sodium bicarbonate were purchased from Sigma-Aldrich (San Luis, EUA); formvar from Ted Pella INC (Redding, USA); high glucose Dulbecco's Modified Eagle Medium (DMEM) with or without phenol red, fetal bovine serum (FBS), penicillin, streptomycin, and trypsin/EDTA from Gibco/Thermo Fisher Scientific (Waltham, EUA); crystal violet dye and ethanol, from Merk (Darmstadt, Germany); and all plastic material for cell culture from Sarstedt (Nümbrecht, Germany). Ultrapure water (18.2 M Ω cm, Millipore) was used in the preparation of all solutions and all washing steps.

2.4.2 | Nanoparticles stability in a biological environment

Nanoparticles suspensions were mixed with a complete cell culture medium (DMEM without phenol red containing 10% FBS) or water, resulting in a final concentration of 4 μ g/mL. Mixtures were maintained for 3 days at simulated cell culture conditions (37°C, 5% CO₂ in humidified atmosphere), and then photographed and observed under a 10 \times objective of a light microscope to observe aggregates formation.¹⁶

2.4.3 | Cell culture and in vitro exposure

Murine fibroblasts Balb/3T3 clone A31 (ATCC, CCL-163), macrophages RAW 264.7 (BCRJ, 0212), and melanoma cells B16-F10 (BCRJ, 0046) were cultivated in high glucose DMEM, supplemented with 10% FBS, 0.25 μ g/mL of penicillin/streptomycin, and 1.57 g/L of sodium bicarbonate. For macrophages, the FBS was heat-inactivated at 56°C for 30 min before use. All cell lines were maintained in a humidified incubator at 37°C and 5% CO₂, and subcultured upon reaching a maximum confluence of 80%. Cell lines identity was monitored by their respective morphology, growth pattern, and pellet color since melanoma cells produce melanin pigments. Cells for experiments were used for no more than 5 passages.

Stock nanoparticle suspensions were kept in pure ethanol, therefore were considered sterile. The most concentrated dispersion of each nanoparticle was prepared by diluting the stock in water to a final concentration of 20 μ g/mL of nanoparticles and 2.5% ethanol so that after diluting 5 times in the cell culture media the ethanol concentration was 0.5%. From that, dispersions containing different nanoparticles concentrations were prepared from serial dilutions (1:10 ratio¹⁷) in 2.5% ethanol solution in water (to maintain the ethanol concentration constant), which was also used as vehicle control for all

biological assays. The amount of dispersion added to the cell culture medium accounted for 20% of the final volume, resulting in nanoparticle concentrations ranging from 0.4 μ g/mL to 4 μ g/mL.

2.4.4 | Biocompatibility screening

Cells were seeded into 96-well plates at the following densities (cells/cm²): 2.08 \times 10⁴ Balb/3T3, 1.56 \times 10⁴ RAW 264.7, and 5.21 \times 10² B16-F10. Nanoparticles or vehicle control were added after 24 h, and cells were cultivated in their presence for 72 h. Cell viability was determined using the neutral red assay¹⁸: cells were incubated with 0.04 mg/mL neutral red solution for 2 h, retained dye into cells was eluted using 50% ethanol and 1% glacial acetic acid in the water, and absorbance was read at 540 nm wavelength. Cell density/proliferation was evaluated by crystal violet staining¹⁹: cells were incubated with 0.25 mg/mL crystal violet solution for 20 min, the dye was eluted using 33% glacial acetic acid in the water, and absorbance was read at 570 nm. For all colorimetric assays, absorbances were measured using an EpochTM Microplate Spectrophotometer (BioTek Instruments). Before crystal violet dye elution, representative images of each experimental group were obtained using an inverted light microscope. For nanoparticle uptake estimation, the neutral red absorbance was normalized by the cell number (crystal violet absorbance) of each sample.^{16,20,21}

2.4.5 | Statistics

At least 4 independent experiments were performed for biocompatibility screening. Either ROUT or Grubbs tests were applied to identify outliers. A threshold of 30% reduction in any of the studied biocompatibility parameters compared to control was considered biologically significant cytotoxicity.²²

3 | RESULTS

3.1 | Morphological, structural, and chemical results

Previous results from samples as synthesized¹⁵ reveal that nanoparticles are nucleated with sizes between 3–7 nm. The organic additives coat the nucleated nanoparticles and then form spherical clusters with sizes between 20–40 nm, later these spherical clusters form approximately flat clusters with sizes from 0.8 to 2 μ m. This process takes place during the dripping time of NaBH₄ in the solution with metal salts and organic additives as shown schematically in Figure 1B.

TEM results reveal the spherical clusters evolution with thermal annealing temperature. In Figure 2 it is possible to observe that at 400°C the particles that were nucleated grew by reducing the spacing between them and thus did not change the spherical agglomerates average size, that is, 30 nm. At 600°C, the nucleated nanoparticles

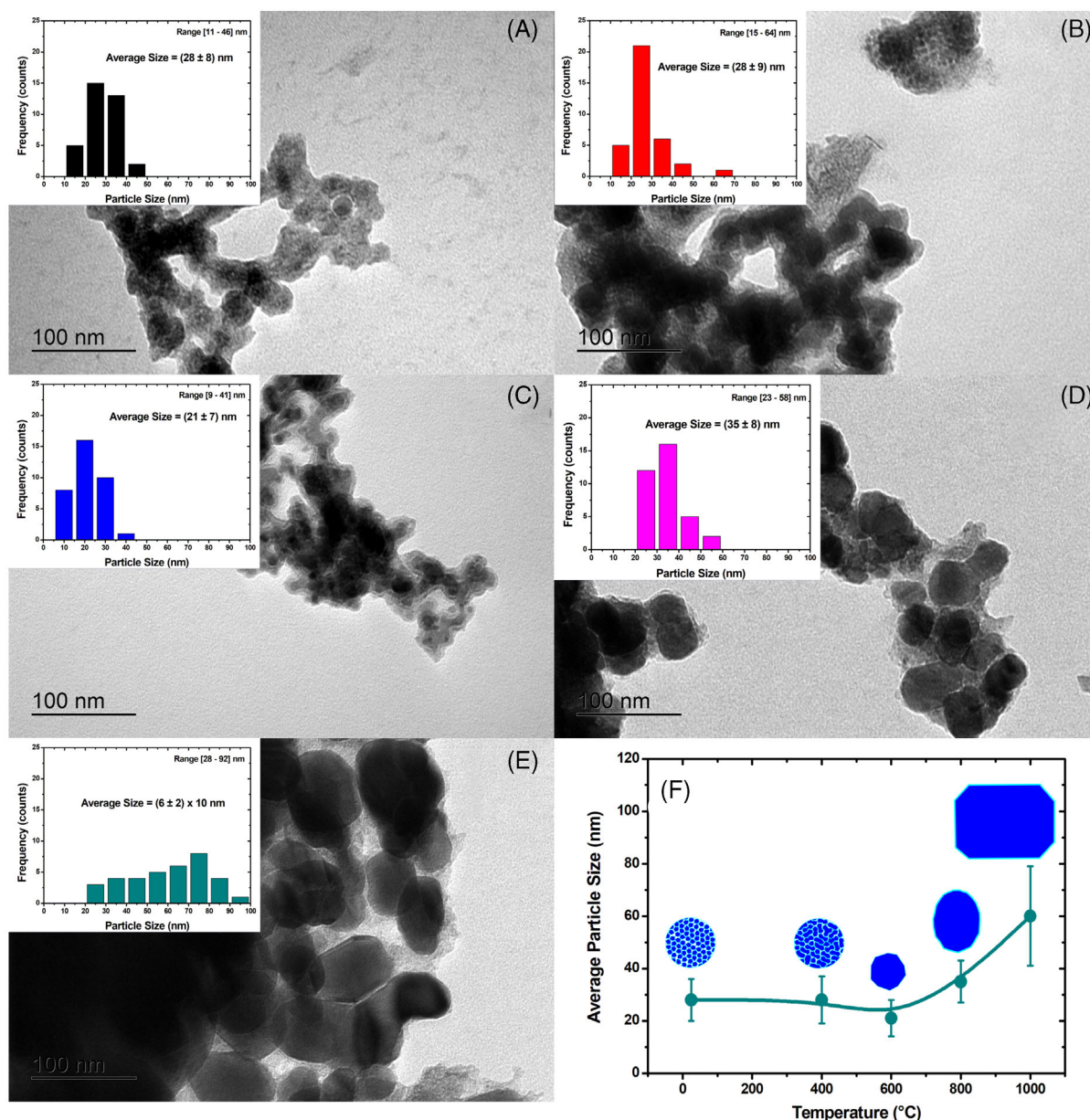


FIGURE 2 TEM results for NiFeMo nanoparticles (NP) centrifuged at 4–5 krpm. The scale bar is the same for figures (A) to (E) with a value of 100 nm. (A) NP as synthesized; (B) NP annealed at 400°C; (C) NP annealed at 600°C; (D) NP annealed at 800°C; (E) NP annealed at 1000°C; (F) NPs average sizes evolution with the annealing temperature. The histograms of sizes distribution are as inserts in the respective figures of (A) to (E). The curve is just a guide for the eyes.

cohesion into a single particle coated with a low electronic contrast layer occurs, accompanied by a significant reduction in nanoparticles average size, going to 20 nm. When the thermal annealing temperature was 800°C the particles grew and assume an oval shape with an average size of 38 nm. At 1000°C the growth was quite noticeable reaching the average size of 60 nm in wide size distribution. In addition, it was possible to observe plane faces in particles contours. This thermal evolution is shown in Figure 2F. Structural aspects measured by SAED report an amorphous structure for the sample as synthesized. As the sample was annealed at 400°C some long-range order appears to be established.

At 600°C the nanoparticles were more crystalline with better-defined rings. At the annealing temperature of 800°C, the particles grew, presented a well-defined crystalline structure, and intense but discontinuous rings were formed. At 1000°C the particles were even larger with the crystallinity also very well defined, to the point that it was possible to register the long-range ordering with the (100) plane register. These results confirm that NiFeMo alloy has the same crystal structure as Ni₃Fe alloy, which is cubic with $a = 0.3545$ nm and space group Pm3m ($n^{\circ}221$) (PDF n° 88-1715), but with a lattice parameter of 0.3620 nm indicating an expansion of approximately 2%. Another aspect to be recorded is the

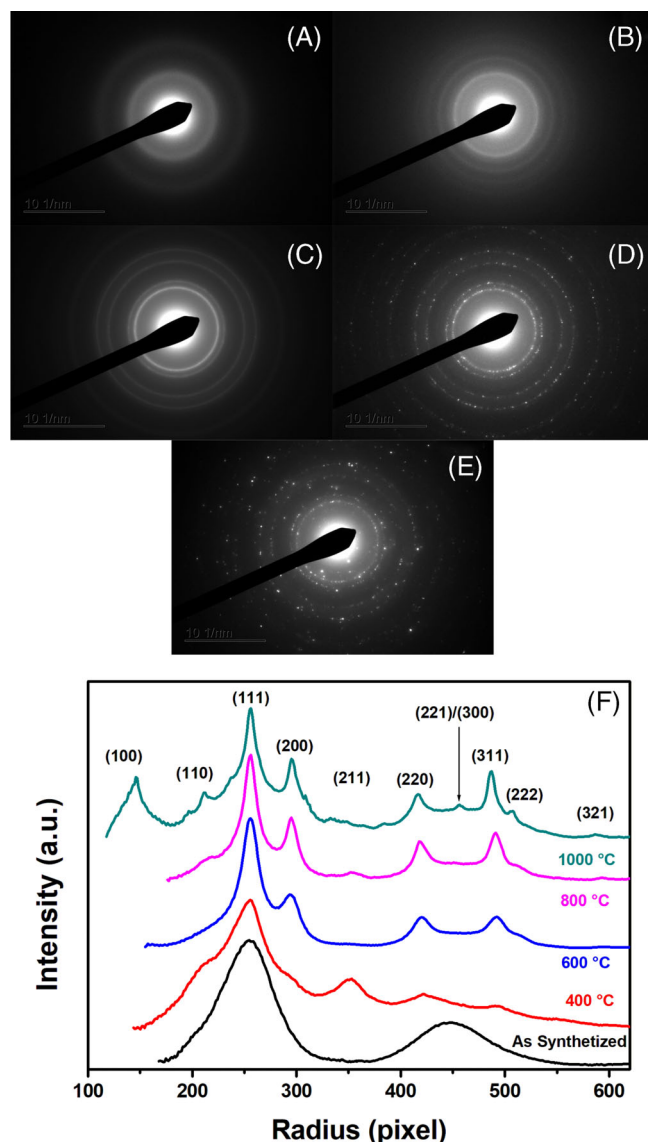


FIGURE 3 SAED results of NiFeMo nanoparticles (NP) centrifuged at 4–5 krpm. (A) NP as synthesized; (B) NP annealed at 400°C; (C) at 600°C; (D) at 800°C; (E) at 1000°C (F) Diffractions intensity profiles are shown in figures 3 (A) to (E). The profiles were obtained through the Radial Profile plugin in the Image J software version 1.52 p.

increase in nanoparticle agglomeration to 1000°C, which is possible to cause during thermal annealing. Figure 3 shows these results. In the case of Figure 3F the diffraction rings intensity profiles were normalized at the maximum intensity of each profile and shifted vertically for better visualization.

The elemental chemical analysis is shown in Table I. Other elements foreign to the synthesis were not detected, only Ni, Fe, Mo, C, and O. As it was possible to observe, the O and C contents were reduced with increasing annealing temperature. Another important aspect is that when disregarding the C and O contents and renormalizing the data only for Ni, Fe, and Mo and still calculating the average value presented as a function of the annealing temperature, the

following values were found: (78 ± 2) Ni wt.%, (19 ± 1) Fe wt% and (3.3 ± 0.9) Mo wt%.

These results suggest a good stability of the metals that make up the nanoparticles for different temperatures.

3.2 | Magnetic measurements

Characterization of the magnetic properties at room temperature was performed for the nanoparticles as-synthesized and for the nanoparticles that were subjected to different temperatures of thermal annealing. These results are shown in Figure 4. Subtle changes are noticeable up to 600°C. Increasing the annealing temperature M_s increases significantly and in nanoparticles thermally annealed at 1000°C, M_s value increases almost 6 times. The M_r also reaches its lowest value when the thermal annealing temperature was 1000°C, being reduced by 30%, concerning M_r for the nanoparticles as-synthesized. H_c values also suffered great variations as seen in Figure 4D. These measurements showed a maximum annealing temperature of 800°C followed by a precipitous drop in temperature of 1000°C. The value of H_c in nanoparticles thermally annealed at 1000°C is small enough to envision far-reaching biomedical applications.

3.3 | Characterization of cell viability

3.3.1 | Nanoparticles characterization and stability in a biological environment

Two groups of nanoparticles were selected by the differential centrifugation technique for the biological assays. These groups were selected through two sets of centrifuge speeds, 1–2 krpm, and 4–5 rpm. These two groups of nanoparticles were placed in a cell culture medium to verify if other interactions occurred that would increase nanoparticles agglomeration in addition to that observed in the synthesis. Transmission electron microscopy measurements (not shown) revealed the agglomerates size distribution in these two centrifuge speed ranges.

Centrifugation speed of 1–2 krpm precipitated agglomerates with an average size of (1.3 ± 0.3) μm , and for the speed of 4–5 krpm the average size was (0.14 ± 0.06) μm . Furthermore, no particle precipitates were observed by light microscopy in cell culture medium (data not shown). Therefore, it is evident that cell culture medium chemical composition, specially FBS presence, does not induce evident nanoparticles aggregation, precipitation, or sedimentation when compared to those incubated in water under the same environmental conditions.

3.3.2 | Nanoparticles biocompatibility in vitro

The nanoparticles developed in this study are intended to be applied as antitumor therapeutic tools. Therefore, we investigated their

Temperature (°C)	Elements				
	C (wt.%)	O (wt.%)	Ni (wt.%)	Fe (wt.%)	Mo (wt.%)
As-Synthesized	11.0	42.4	37.4	8.0	1.2
400	11.2	43.0	34.4	9.1	2.2
600	6.0	33.1	43.0	10.7	1.6
800	5.4	32.1	48.5	11.8	2.2
1000	4.8	30.9	51.3	11.3	1.7

TABLE I Results of EDS measurements for nanoparticles centrifuged between 4–5 krpm at different annealing temperatures.

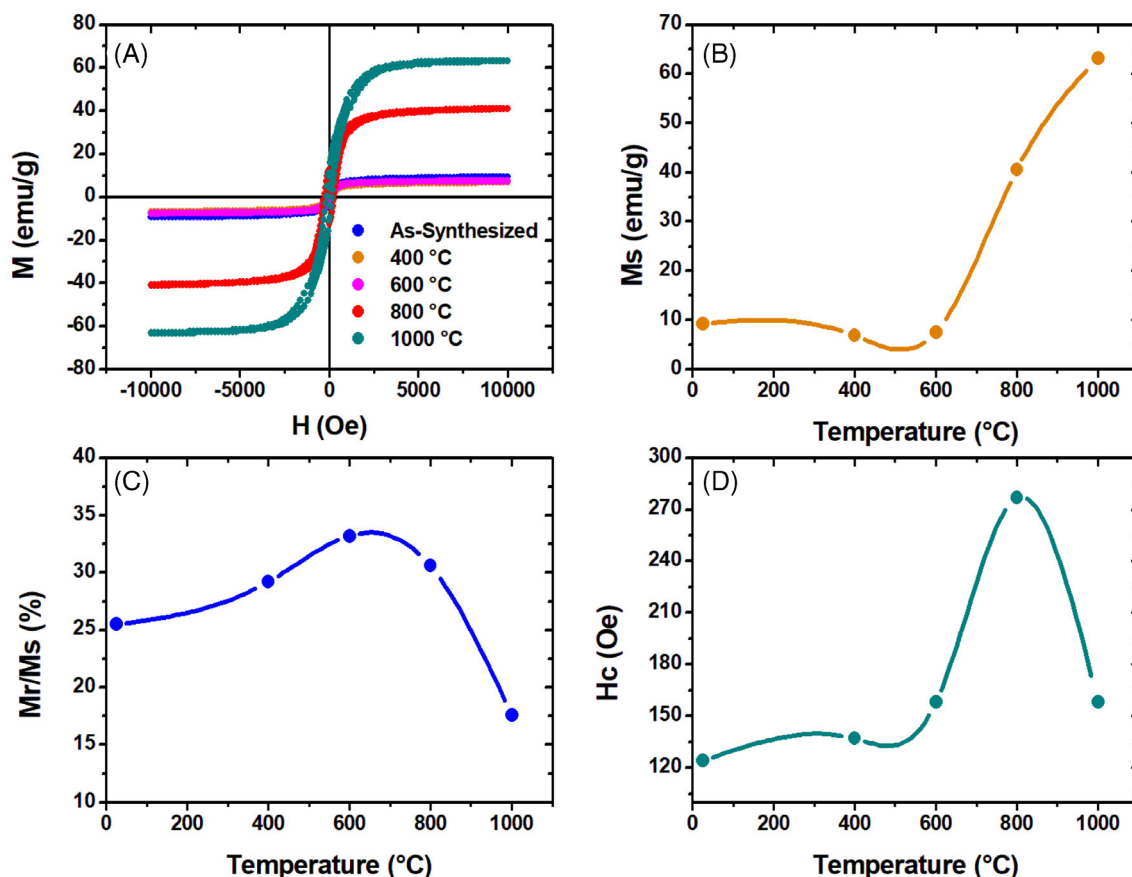


FIGURE 4 (A) Magnetic measurements of magnetization (M) versus applied external magnetic field (H), performed at 25°C for the nanoparticles as-synthesized and thermally annealed at different temperatures; (B) Ms values for different annealing temperatures; (C) percentage values of Mr relative to Ms values; (D) Hc values for samples annealed at different temperatures. The lines are just a guide for the eyes.

biocompatibility with not only a melanoma model but also with non-tumorigenic cells, namely fibroblasts and macrophages, which are the main representatives of the tumor microenvironment^{23,24} as well as important components of normal tissues.^{25,26} Two biocompatibility indicator assays were used: crystal violet staining for cell density/proliferation, and neutral red uptake for cellular endomembrane viability. For that, fibroblasts, macrophages, and melanoma cells were exposed to eight nanoparticles concentrations (0.4 µg/mL to 4 µg/mL) or vehicle control (0.5% ethanol, the limit recommendation since higher concentrations of organic solvent vehicles might be cytotoxic^{17,22}) for 72 h. A threshold of 30% reduction in any of the studied parameters compared to the vehicle control (i.e., below the pink filled space in

Figure 5) was considered biologically significant cytotoxicity.²² Results show that nanoparticles concentration of up to 0.4 µg/mL does not significantly interfere with cell density or viability, regardless of cell type or nanoparticles size. On the other hand, the higher concentration tested (4 µg/mL) reveals that Nps 1–2 krpm (1.3 µm) were more cytotoxic to all cell lines, being able to reduce both cell density (by 59% for fibroblasts, 61% for macrophages, and 36% for melanoma cells) and viability (by 49% for fibroblasts, 33% for macrophages, and 56% for melanoma cells) to below the acceptable limit. Whilst, 4 µg/mL of Nps 4–5 krpm (0.14 µm) only reduced macrophages density and melanoma cells viability, both by 32%, not surpassing the biocompatibility threshold for the other cells/parameters (Figure 5A–a, b, d, e, g, h).

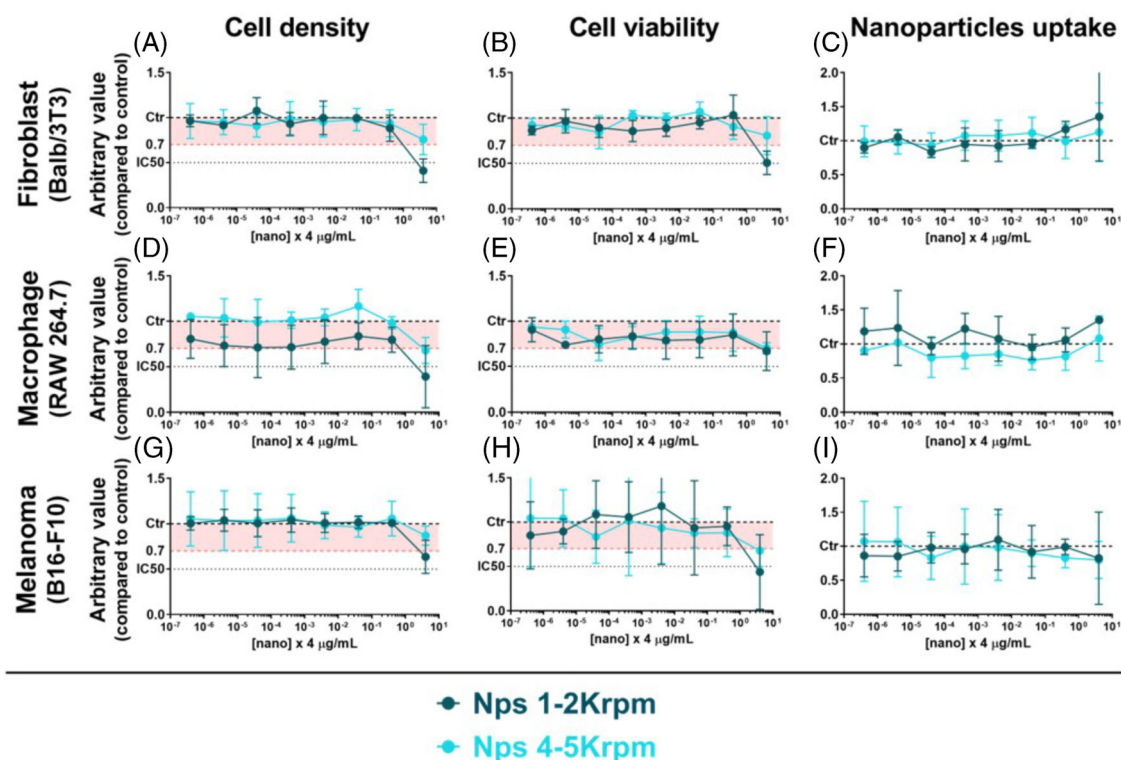


FIGURE 5 Cells were cultivated in the presence of two sizes (Nps 1–2 krpm – 1.3 μm, and Nps 4–5 krpm – 0.14 μm) in eight nanoparticles concentrations for each size (0.4, 4, 40 pg/mL; 0.4, 4, 40 ng/mL; 0.4, and 4 μg/mL) or the vehicle control (ethanol 0.5%) for 72 h. Cells were colorimetrically assayed for cell density (by crystal violet dye staining) and cell viability (by neutral red dye uptake) determination. Results are shown as mean ± SD and represent at least four independent experiments performed in quadruplicate. All nanoparticle exposed groups were normalized by the vehicle control (black dashed line, normalized as 1) of each respective experiment. The red dotted line and pink filled space show the interval of 0%–30% reduction of each parameter. The IC50 (black dotted line) shows the reduction of each parameter by 50%. For estimation of nanoparticle uptake, neutral red absorbance was normalized by each sample cell number.

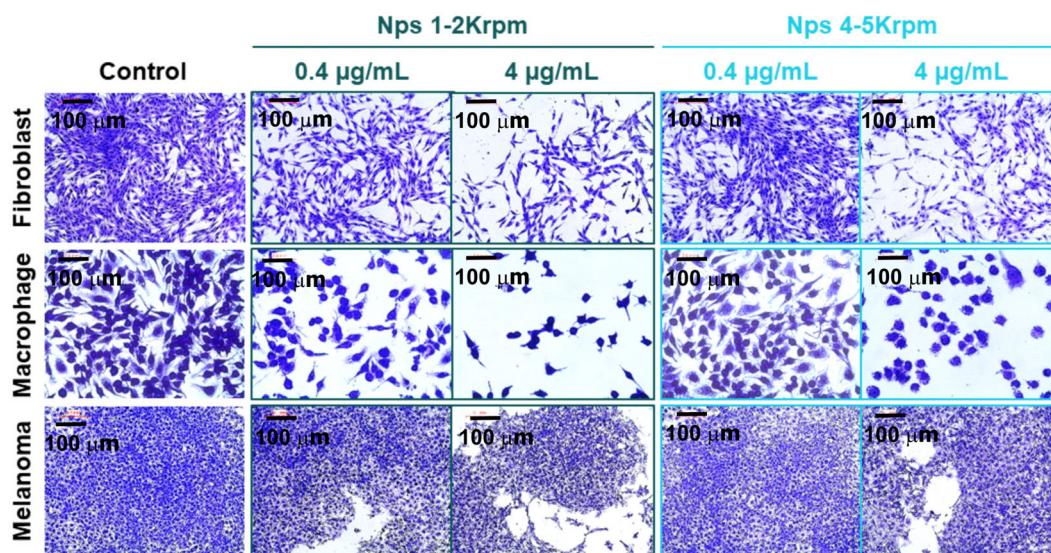


FIGURE 6 Cells were cultivated in the presence of two nanoparticle concentrations or the vehicle control (ethanol 0.5%) for 72 h. Cells were stained using crystal violet dye, and then representative images of each experimental group were obtained by phase contrast microscopy (scale bar = 100 μm).

Interestingly, melanoma cells are less sensitive to Nps 1–2 krpm's (at 4 $\mu\text{g}/\text{mL}$) reduction of cell density (Figures 5A-g, and 6) than the non-tumorigenic cells, which slightly overcome the IC_{50} at such condition (Figures 5A-a, d, and 6). Figure 6 shows the light microscopy images of the three sets in the control condition and exposed to nanoparticles with two different concentrations and two different average sizes.

4 | DISCUSSION

The synthesis of nanoparticles composed of NiFeMo was performed by the technique of chemical coprecipitation in the presence of organic additives. In Figure 1B the mechanism of agglomerates formation is schematized. First, very small nanoparticles (3–7 nm) coated with organic molecules were nucleated. These small nanoparticles formed spherical aggregates (30–40 nm) where it was possible to observe the nucleated particles inside them spaced 1–2 nm apart. Subsequently, these spherical aggregates assemble forming large agglomerated plates (0.5–2 μm). With each drop of NaBH_4 new particles were nucleated and the formation process of spherical aggregates and large agglomerates was in progress. Therefore, at the synthesis end, a wide size distribution were present in the final solution.

In previous work¹⁵ the morphological diversity between precipitates and supernatants was demonstrated. However, both samples were structurally amorphous. From the point of view of magnetic properties, the samples showed a low saturation field, a relative remanence of 22%, and a sufficiently low coercive field for future applications. Because of these results, two actions were taken: to change the composition and to promote the nanoparticles crystallization. After cleaning, the nanoparticles were separating them into two groups of different sizes, by differential centrifugation. Then the NPs of these two groups were subjected to thermal annealing at different temperatures. The results for particles centrifuged in the range of 4–5 krpm are shown in Figure 2.

From the TEM results, it was possible to describe how the nanoparticles morphology evolution occurs with the increase in the annealing temperature. Whereas growth occurs by the nanoparticles coalescence as described by Yacaman et al.²⁷ diffusion coefficient values at each annealing temperature were calculated. From these values, an Arrhenius plot (not shown) was made. The results provided an activation energy $E_a = (0.60 \pm 0.04)$ eV/atom and a diffusion coefficient prefactor $D_0 = (5 \pm 3) \times 10^{-16}$ m^2/s . Comparing the results with the literature data, it is observed that the value of E_a is compatible with the activation energy of Ni in Fe (0.62 eV/atom)²⁸ and the value obtained for the diffusion coefficient is similar to that found for Pt structures (3.3×10^{-15} m^2/s).²⁹

From a structural point of view, the as-synthesized samples are amorphous with two broad and low-intensity rings with the maximum close to where the rings positions of planes (111) and (220) would correspond, according to the profiles intensity of SAED measurements, shown in Figure 3F.

As the annealing temperature increases, the nanoparticles grow and become more organized, increasing the long-range order. The result of this fact is reflected in the electron diffraction pattern obtained in the annealed nanoparticles at 1000°C. At the annealing temperature of 1000°C the long-range crystallinity is established and it was possible to observe the (100), (110), (111), (200), (220), (221) or (300) planes, (311), (222), and (321). This crystallinity evolution with the annealing temperature is in complete agreement with the morphology thermal evolution shown in Figure 2. It is important to note that no other crystalline phases were observed in the SAED measurements.

The measurements referring to elemental chemical analysis by the EDS technique for nanoparticles centrifuged in the range of 4–5 krpm, show that no elements other than Ni, Fe, Mo, C, and O were observed. This indicates that there are no salt chlorides and sodium residues from the other reagents. It is also possible to observe that C and O contents are reduced with the annealing temperature increase. However, complete elimination of C and O in the samples were not detected. This can be explained by the detection of C and O from atmospheric contamination by hydrocarbons and water vapor present in the atmosphere. This is supported by the fact that at temperatures of 800 and 1000°C, morphologically, no oxide phases were detected, which would certainly present a low contrast in the TEM images. At these temperatures, any oxide phase would have crystallized, and by the SAED technique, it was also not detected. At lower temperatures, the presence of these phases is not ruled out, but in an amorphous state. This contamination is superficial, but when it comes to the surface of nanoparticles this effect can be very large due to their huge surface area. From the results, we can also verify that the stoichiometric proportion of the alloy does not vary significantly with temperature.

Regarding the magnetic properties, the samples showed a great change as the NPs centrifuged between 4–5 krpm became crystalline. The magnetic moment changes from 0.10 μ_B in the as-synthesized sample to 0.67 μ_B for the annealed sample at 1000°C. This proves the importance of the effective anisotropy constant due to the nanoparticles crystallization, that is, the magnetic ordering increases the nanoparticles magnetic moment as predicted.³⁰ The remanence also shows a relative reduction of 31% compared to as-deposited nanoparticles. The coercive field measurements H_c show a high value at 800°C followed by an abrupt drop at 1000°C, this behavior can be explained by the transition from magnetic single domains to magnetic multiple domains. According to the literature,¹⁴ the value of H_c depends directly on the effective anisotropy constant and inversely on the saturation magnetization. However, the effective anisotropy constant grows with d^6 , where d is the mean particle diameter when the nanoparticle sizes harbor a single domain. This dependence is drastically altered when the particles size increases and starts to house multiple magnetic domains. In this situation, the effective anisotropy constant varies with d^{-1} . Therefore, what is observed in Figure 4D is the passage of nanoparticles with single domains to multiple domains. In short, the increase in crystallinity and particle size increases saturation magnetization, being an important aspect for hyperthermia magneto

applications where external magnetic fields are applied relatively far from nanoparticles. The increase in the size of these nanoparticles with the temperature showed the fall of the coercive field, due to 60 nm these nanoparticles change from magnetic mono-domains to magnetic multi-domains. This facilitates the reversal of magnetization when alternate magnetic fields are applied. Finally, there is a decrease in remanence magnetization that reduces the possibility of agglomeration of these nanoparticles in the absence of an external magnetic field, enhancing future biomedical applications.

Regarding the biological assays, nanoparticles synthesized by coprecipitation were produced without any type of coatings such as Au, SiO₂, or polymers with two different size distributions 1–2 krpm (1.3 μm) and 4–5 krpm (0.14 μm). The interaction of nanoparticles with proteins from biological environments can easily lead to the formation of a protein corona around the nanoparticles surface, which can directly affect their state of aggregation, interaction with cells and tissues, cellular uptake, and consequently, their biological effects.^{31,32} Therefore, to understand this effect on the nanoparticles stability, we exposed them to a protein-rich cell culture medium and incubated them under the complex environmental conditions of cell culture (optimal temperature, humidity, pH, salt concentration, etc.) for 3 days, which represents the period of cellular exposure for biocompatibility assays. Results revealed that the culture microenvironment especially in the presence of FBS does not affect NPs, which was confirmed by the absence of visible precipitate under light microscopy (data not shown).

Nanoparticles cytotoxicity is widely studied^{2,36–38}; however, depending on nanoparticle material, size, shape, and coating, as well as cell type, incubation periods, and concentration used results can be variable. To the best of our knowledge, here we describe the first results on NiFeMo alloy nanoparticles biocompatibility, and we were able to show in vitro a diversity of effects depending on the concentration and cell type.

We hypothesized that the distinct biological effects of NPs 1.3 μm and NPs 0.14 μm may be due to quantitative differences in cellular uptake. Cells generally internalize nanoparticles through processes of endocytosis, which consists of the vesicle formation on the cell surface, followed by their internalization and acidification to digest the incorporated material.^{32–35} Here, we leverage the principle behind the neutral red assay to indirectly estimate the cellular uptake of nanoparticles. The dye is neutral at physiological pH, which allows it to diffuse freely across cell membranes, but becomes protonated and retained within acidic vesicles. Therefore, by dividing the absorbance of incorporated neutral red dye by the crystal violet stain absorbance (related to the number of cells), we compared the amount of acidic intracellular vesicles generated by each cell due to the absorption of nanoparticles.^{18,20,21} Although not statistically significant, exposure of fibroblasts and macrophages to the three highest concentrations of NPs 1–2 krpm shows a trend of increasing cellular uptake in a concentration-dependent manner, where 4 μg/mL increases by 35% for both cell lines. (Figure 5C,F). Considering that the size of nanoparticles is a key characteristic for their interaction with cells

and, consequently, for their internalization,^{39,40} this effect may partially explain why nanoparticles of this size are more effective in reducing the density/proliferation of non-tumorigenic cells (Figure 5A,D). Melanoma cells, on the other hand, show a less pronounced reduction in cell density (Figure 5G), probably because they internalized fewer nanoparticles (Figure 5I).

Taken together, these results show that NiFeMo nanoparticles of both sizes are non-cytotoxic to non-tumorigenic cells up to 0.4 μg/mL, while at higher concentrations 1–2 krpm Nps (1.3 μm) affects cells density and viability. It is hoped that such knowledge can guide future studies toward a biological application.

5 | CONCLUSION

In summary nanoparticles (NPs) were synthesized by co-precipitation in the presence of organic additives. From these NPs two studies were carried out. The first evaluated the morphology evolution, crystal structure, chemical composition, and magnetic properties measured at room temperature. The second study investigated the cell viability of fibroblasts, macrophages, and melanoma exposed to as-synthesized NiFeMo NPs incubated for 72 h. The results showed that the NPs increased by about 114% accompanied by a well-consolidated crystal structure at 1000°C of the cubic type with $a = 0.362$ nm and space group Pm3m ($n^{\circ}221$). Chemically, the C and O contents reduction was observed with increasing annealing temperature. The magnetic properties also underwent major changes such as a 578% increase in saturation magnetization and a 29% reduction. For cell viability assays, it was shown that at concentrations up to 0.4 μg/mL, NiFeMo NPs are not cytotoxic to non-tumorigenic cells (Balb/3T3 fibroblasts and RAW 264.7 macrophages) or tumor cells (B16-F10 melanoma). Increased uptake of NPs was also observed with increasing concentration for non-tumorigenic cells. These results may contribute one more option of magnetic nanoparticles for future biomedical applications.

ACKNOWLEDGMENTS

The authors would like to thank the UFPR Electronic Microscopy Center for its use and access to the equipment.

DATA AVAILABILITY STATEMENT

Data sharing not applicable to this article as no datasets were generated or analysed during the current study.

ORCID

Ney Mattoso  <https://orcid.org/0000-0001-7486-0722>

REFERENCES

1. Curtis A, Wilkinson C. Nanotechniques and approaches in biotechnology. *Trends Biotechnol.* 2001;19:97–101.
2. Wei H, Hu J, Wang J, Gao X, Qian X, Tang M. Superparamagnetic iron oxide nanoparticle: cytotoxicity, metabolism, and cellular behavior in biomedicine applications. *Int J Nanomedicine.* 2021;16:6097–6113. doi:10.2147/IJN.S321984

3. Rybka JD. Radiosensitizing properties of magnetic hyperthermia mediated by superparamagnetic iron oxide nanoparticles (SPIONs) on human cutaneous melanoma cell lines. *Reports Pract Oncol Radiother.* 2019;24:152-157. doi:10.1016/j.rpor.2019.01.002
4. Tong HI, Kang W, Shi Y, Zhou G, Lu Y. Physiological function and inflamed-brain migration of mouse monocyte-derived macrophages following cellular uptake of superparamagnetic iron oxide nanoparticles-implication of macrophages drug delivery into the central nervous system. *Int J Pharm.* 2016;505:271-282. doi:10.1016/j.ijpharm.2016.03.028
5. Kanetaka H, Liu G, Li Z, et al. TiO₂ microspheres containing magnetic nanoparticles for intra-arterial hyperthermia. *J Biomed Mater Res B: Appl Biomater.* 2017;105B:2308-2314. doi:10.1002/jbm.b.33765
6. Nguyen D, Pham BTT, Huynh V, et al. Monodispersed polymer encapsulated superparamagnetic iron oxide nanoparticles for cell labeling. *Polymer.* 2016;106:238-248. doi:10.1016/j.polymer.2016.08.06
7. Yao D, Liu N, Mo B. Assessment of proliferation, migration and differentiation potentials of bone marrow mesenchymal stem cells labeling with silica-coated and amine-modified superparamagnetic iron oxide nanoparticles. *Cytotechnology.* 2020;72:513-525. doi:10.1007/s1061-020-00397-5
8. Yuan M, Wang Y, Qin YX. SPIO-Au core-shell nanoparticles for promoting osteogenic differentiation of MC3T3-E1 cells: concentration-dependence. *J Biomed Mater Res A.* 2017;105A:3350-3359. doi:10.1002/jbm.a.36200
9. Elkhenany H, Elkodous MA, Ghoneim NI, et al. Comparison of different uncoated and starch-coated superparamagnetic iron oxide nanoparticles: implications for stem cell tracking. *Int J Biol Macromol.* 2020;143:763-774. doi:10.1016/j.ijbiomac.2019.10.031
10. Shabani M, Sebnouri E, Hassanzadeh-Tabrizi SA, Bakhsheshi-Rad HR. Solution plasma synthesis of polymer-coated NiFe₂O₄ nanoparticles for hyperthermia application. *J Mater Eng Perform.* 2022;32:2165-2182. doi:10.1007/s11665-022-07268-4
11. Cambre Mh Holl NJ, Wang B, Harper L, et al. Cytotoxicity of NiO and Ni(OH)₂ nanoparticles is mediated by oxidative stress-induced cell death and suppression of cell proliferation. *Int J Mol Sci.* 2020;21:2355-23576. doi:10.3390/ijms21072355
12. Boothby OL, Bozorth RM. A new magnetic material of high permeability. *J Appl Phys.* 1947;18:173-176. doi:10.1063/1.1697599
13. Chicinas I, Pop V, Isnard O. Synthesis of Superalloy powders by mechanical alloying. *J Mater Sci.* 2004;39:5305-5309. doi:10.1023/B:JMSE.0000039234.58490.78
14. Shen YP, Hng HH, Oh JT. Synthesis and characterization of high-En ball milled Ni-15%Fe-5%Mo. *J Alloy Compound.* 2004;379:266-271. doi:10.1016/j.jallcom.2004.02.032
15. Muchenski F, Mattoso N. Synthesis and characterization of Ni₇₉Fe₁₅Mo₆ nanoparticles produced by Co-precipitation in the presence of organic additives. *J Mater Sci Eng B.* 2021;11:89-97. doi:10.17265/2161-6221/2021.7-9001
16. Gonçalves JP, de Oliveira CC, Trindade ES, Riegel-Vidotti IC, Vidotti M, Simas FF. In vitro biocompatibility screening of a colloidal gum Arabic-polyaniline conducting nanocomposite. *Int J Biol Macromol.* 2021;173:109-117. doi:10.1016/j.ijbiomac.2021.01.101
17. ICCVAM. ICCVAM-Recommended Test Method Protocol BALB/c 3T3 NRU Cytotoxicity Test Method, in: ICCVAM Test Method Eval. Rep. Vit. Cytotox. Test Methods Estim. Start. Doses Acute Oral Syst. Toxic. Tests, 2006.
18. Repetto G, del Peso A, Zurita JL. Neutral red uptake assay for the estimation of cell viability/cytotoxicity. *Nat Protoc.* 2008;3:1125-1131. doi:10.1038/nprot.2008.75
19. Gillies RG, Didier N, Denton M. Determination of cell number in monolayer cultures. *Anal Biochem.* 1986;159:109-113.
20. Gonçalves JP, da Cruz AF, Nunes AM, et al. Biocompatible gum arabic-gold nanorod composite as an effective therapy for mistreated melanomas. *Int J Biol Macromol.* 2021;185:551-561. doi:10.1016/j.ijbiomac.2021.06.172
21. Gonçalves JP, da Cruz AF, de Barros HB, et al. Beyond gold nanoparticles cytotoxicity: potential to impair metastasis hallmarks. *Eur J Pharm Biopharm.* 2020;157:221-232. doi:10.1016/j.ejpb.2020.10.019
22. International Organization for Standardization. Tests for in vitro cytotoxicity, in: Biol. Eval. Med. Devices. 2009 <http://nhiso.com/wp-content/uploads/2018/05/ISO-10993-5-2009.pdf>
23. Xing F, Saidou J, Watanabe K. Cancer associated fibroblasts (CAFs) in tumor microenvironment. *Front Biosci.* 2010;15:166-179. doi:10.2741/3613
24. Chanmee T, Ontong P, Konno K, Itano N. Tumor-associated macrophages as major players in the tumor microenvironment. *Cancers (Basel).* 2014;6:1670-1690. doi:10.3390/cancers6031670
25. Marsh E, Gonzalez DG, Lathrop EA, Boucher J, Greco V. Positional stability and membrane occupancy define skin fibroblast homeostasis In vivo. *Cell.* 2018;175:1620-1633.e13. doi:10.1016/j.cell.2018.10.013
26. Yanez DA, Lacher RK, Vidyarthi A, Colegio OR. The role of macrophages in skin homeostasis. *Pflügers Arch - Eur J Physiol.* 2017;469:455-463. doi:10.1007/s00424-017-1953-7
27. Yacaman JM, Wing CG, Miki M, Yang DQ, Piyakis KN, Sacer E. Surface diffusion on coalescence of Mobile metal nanoparticles. *J Phys Chem B.* 2005;109:9703-9711. doi:10.1021/jp0509459
28. Amento N, Serra A, Osetsky Y. Effect of nickel on point defects diffusion in Fe-Ni alloys. *Acta Mater.* 2017;132:367-373. doi:10.1016/j.actamat.2017.05.010
29. Marcos ML, Velasco JG. Measurement of surface diffusion coefficients in air of columnar structured platinum near room temperature. *Chem Phys Lett.* 1998;283:391-394.
30. Suzuki K, Cadogan JM. Random Magnetocrystalline anisotropy in two-phase nanocrystalline systems. *Phys Rev B.* 1998;58:2730-2739. doi:10.1103/PhysRevB.58.2730
31. Foroozandeh P, Aziz AA. Merging worlds of nanomaterials and biological environment: factors governing protein Corona formation on nanoparticles and its biological consequences. *Nanoscale Res Lett.* 2015;10:221. doi:10.1186/s11671-015-0922-3
32. Kopac T. Protein corona, understanding the nanoparticle-protein interactions and future perspectives: a critical review. *Int J Biol Macromol.* 2021;169:290-301. doi:10.1016/j.ijbiomac.2020.12.108
33. Zhang S, Gao H, Bao G. Physical principles of nanoparticle cellular endocytosis. *ACS Nano.* 2015;9(9):8655-8671. doi:10.1021/acsnano.5b03184
34. Manzanares D, Ceña V. Endocytosis: the nanoparticle and submicron Nanocompounds gateway into the cell. *Pharmaceutics.* 2020;12:371. doi:10.3390/pharmaceutics12040371
35. Patel S, Kim J, Herrera M, Mukherjee A, Kabanov AV, Sahay G. Brief update on endocytosis of nanomedicines. *Adv Drug Deliv Rev.* 2019;144:90-111. doi:10.1016/j.addr.2019.08.004
36. Reddy LH, Ana JL, Nicolas J, Couvreur P. Magnetic nanoparticles: Design and characterization, toxicity and biocompatibility, pharmaceutical and biomedical applications. *Chem Rev.* 2012;112:5818-5878. doi:10.1021/cr300068p
37. Malhotra N, Lee JS, Liman RAD, et al. Potential toxicity on iron oxide Nanoparticles: a review. *Molecules.* 2020;25:3159. doi:10.3390/molecules25143159
38. Sengul AB, Asmatulu E. Toxicity of metal and metal oxide nanoparticles: a review. *Environ Chem Lett.* 2020;18:1659-1683. doi:10.1007/s10311-020-01033-6

39. Kettler K, Veltman K, van de Meent D, van Wezel A, Hendriks AJ. Cellular uptake of nanoparticles as determined by particle properties, experimental conditions, and cell type. *Environ Toxicol Chem.* 2014; 33:481-492. doi:[10.1002/etc.2470](https://doi.org/10.1002/etc.2470)
40. Albanese A, Tang PS, Chan WCW. The effect of nanoparticle size, shape, and surface chemistry on biological systems, annual review. *Biomed Eng.* 2012;14:1-16. doi:[10.1146/annurev-bioeng-071811-150124](https://doi.org/10.1146/annurev-bioeng-071811-150124)

How to cite this article: Muchenski F, Gonçalves JP, Ribeiro YC, et al. Temperature influence on NiFeMo nanoparticles magnetic properties and their viability in biomedical applications. *J Biomed Mater Res.* 2023;1-11. doi:[10.1002/jbm.b.35248](https://doi.org/10.1002/jbm.b.35248)